

Seismic reflection and electrical resistivity imaging reveal pre-Quaternary glaciation in the Rocky Mountains (Unaweep Canyon, Colorado)

Anna Patterson¹, Michael Behm¹, Werner Chwatal², Adrian Flores-Orozco³, Yichuan Wang⁴, and Gerilyn Soreghan⁵

¹School of Geosciences, University of Oklahoma

²AFRY Austria GmbH

³Department of Geodesy and Geoinformation, Vienna University of Technology

⁴Department of Geoscience, University of Calgary

⁵University of Oklahoma

November 23, 2022

Abstract

Unaweep Canyon (Uncompaghe Plateau, Colorado) represents an enigmatic landscape with a complex evolution. Interpretations for its origin have ranged from ancestral fluvial erosion in the late Cenozoic to glacial erosion in the Paleozoic, or some combination thereof, with significant implications for global climatic and large-scale tectonic reconstructions. To address the conflicting interpretations, we acquired a high-resolution seismic reflection profile to investigate the depth, structure, and sedimentary infill in the canyon. The dataset is further complemented with a high-resolution electrical resistivity survey. Integrated with other geophysical and geological data, the results unambiguously demonstrate an overdeepened Precambrian basement with pronounced transverse U-shape and corroborate the hypothesis of a pre-Quaternary glacial origin. Our data constitute the first detailed and high-resolution image of a buried pre-Quaternary glacial valley in North America, and thus have far-reaching implications for our understanding of global ice houses as well as the tectonic conditions enabling preservation of such systems.

1 **Seismic reflection and electrical resistivity imaging reveal pre-Quaternary**
2 **glaciation in the Rocky Mountains (Unaweep Canyon, Colorado)**

3 **Anna Patterson¹, Michael Behm^{1,2}, Werner Chwatal³, Adrian Flores-Orozco⁴, Yichuan**
4 **Wang^{1,5}, and Gerilyn S. Soreghan¹**

5 ¹School of Geosciences, University of Oklahoma, 73019 Norman, OK, US

6 ²Geodata Surveying and Monitoring Group, A-8700 Leoben, Austria

7 ³AFRY Austria GmbH, A-1120 Vienna, Austria

8 ⁴Department of Geodesy and Geoinformation, Vienna University of Technology, A-1040 Vienna,
9 Austria

10 ⁴Department of Geoscience, University of Calgary, Alberta T2N 1N4, Canada

11 **Key Points:**

- 12 • We present the first high-resolution seismic image of a buried paleovalley shaped by
13 alpine glaciation in Earth's pre-Quaternary record.
- 14 • Our data support the hypothesis of late Paleozoic glaciation at latitudes and elevations
15 lower than suggested by current climate models.

16 **Abstract**

17 Unaweep Canyon (Uncompaghre Plateau, Colorado) represents an enigmatic landscape with a
18 complex evolution. Interpretations for its origin have ranged from ancestral fluvial erosion in the
19 late Cenozoic to glacial erosion in the Paleozoic, or some combination thereof, with significant
20 implications for global climatic and large-scale tectonic reconstructions. To address the conflicting

21 interpretations, we acquired a high-resolution seismic reflection profile to investigate the depth,
22 structure, and sedimentary infill in the canyon. The dataset is further complemented with a high-
23 resolution electrical resistivity survey. Integrated with other geophysical and geological data, the
24 results unambiguously demonstrate an overdeepened Precambrian basement with pronounced
25 transverse U-shape and corroborate the hypothesis of a pre-Quaternary glacial origin. Our data
26 constitute the first detailed and high-resolution image of a buried pre-Quaternary glacial valley in
27 North America, and thus have far-reaching implications for our understanding of global ice houses
28 as well as the tectonic conditions enabling preservation of such systems.

29 **1 Introduction**

30 Seismic imaging has been widely used to characterize Quaternary glacial valleys and, together
31 with drilling and other subsurface data, has demonstrated the distinctive propensity for glacial
32 processes to produce not only U-shaped transverse profiles, but uniquely “overdeepened”
33 longitudinal profiles (Preusser et al., 2010; Cook and Smith, 2012). Overdeepening is
34 characterized by closed topographic depressions eroded below fluvial baselevel, and — barring a
35 structural explanation — implies glacial excavation. Overdeepening occurs in cirques, valley
36 outlets of alpine glaciers, and fjords and valleys draining continental ice sheets, related to
37 perturbations in the bed that amplify the action of high-pressure meltwater (Hooke, 1991).
38 Excavation can reach several hundreds of meters (Fiebig et al., 2010).

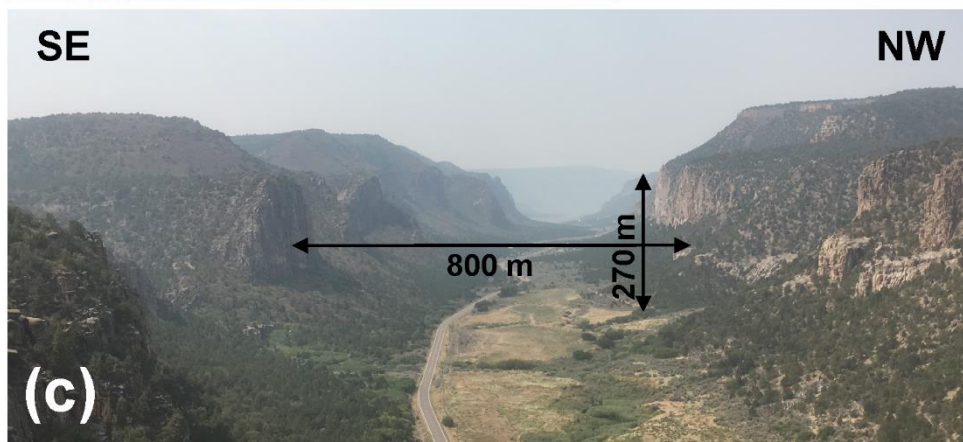
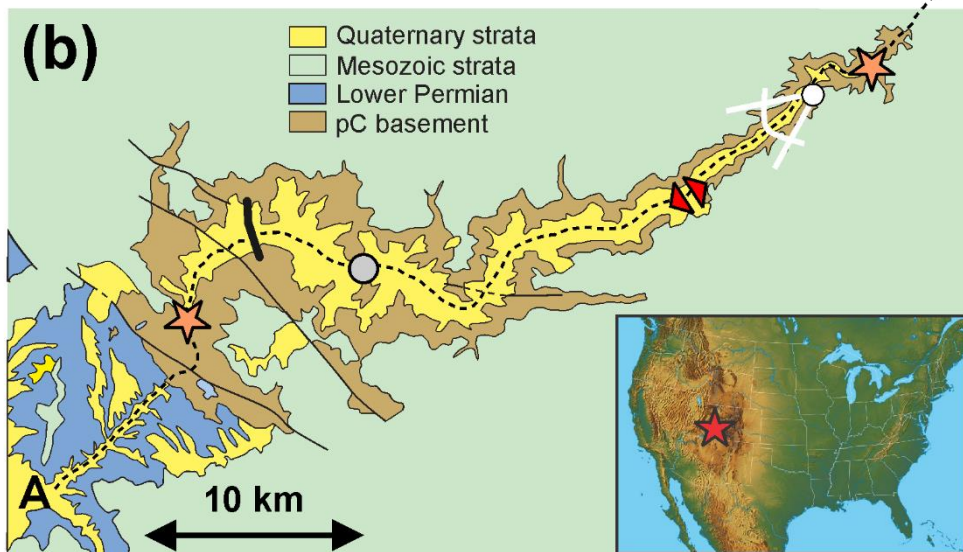
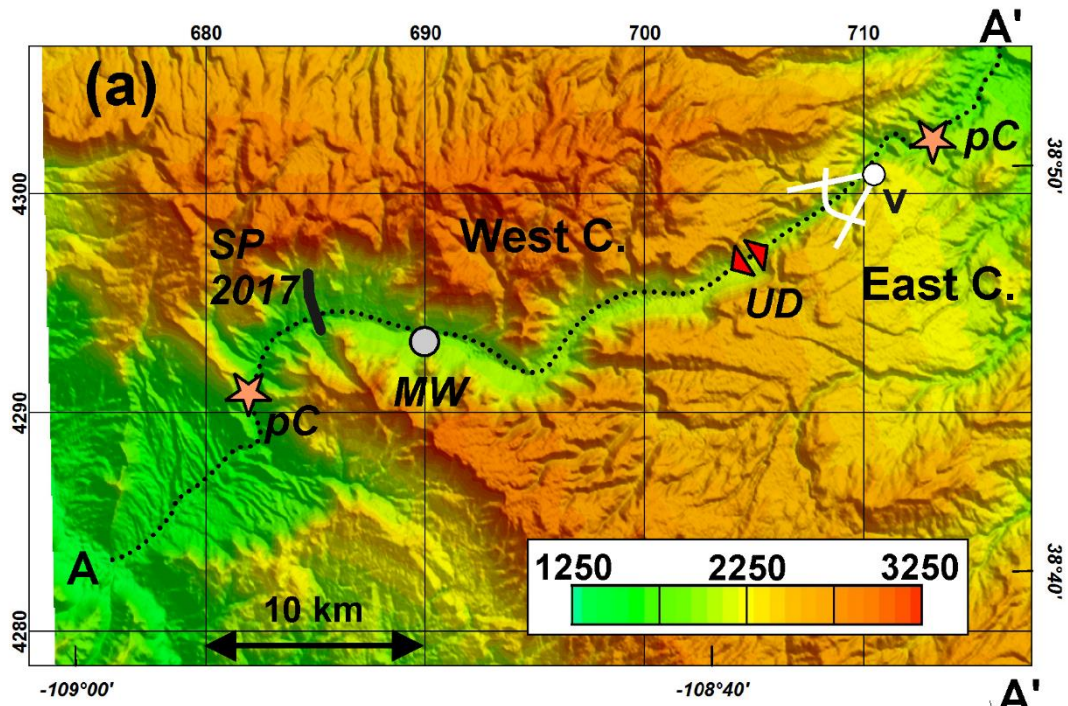
39 Many seismic studies of Quaternary glacial valleys focus on the sediment fill and associated
40 potential for groundwater resources, waste disposal, and hydrocarbon potential in the pre-
41 Quaternary section (e.g., de Franco et al., 2009; Brückl et al., 2010; Bache et al. 2012; Bleibinhaus
42 & Hilberg, 2012; Pomper et al., 2017; Burschil et al., 2018; Bataller et al., 2019). In this paper, we
43 use high-resolution seismic reflection imaging augmented by electrical resistivity data to

44 characterize the bedrock depth and sediment fill of a partially buried valley, Unaweep Canyon, in
45 western Colorado. Although geologic data establish that the canyon hosted an ancestral river as
46 recently as ~1.4 Ma, our results demonstrate substantial overdeepening of a paleovalley that lies
47 concealed beneath a substantial sediment fill, and that cannot be explained by either fluvial erosion
48 or structural disruptions. We use this observation to link the paleovalley to pre-Quaternary (late
49 Paleozoic or Neoproterozoic) glaciation. Our study is the first documentation of a buried pre-
50 Quaternary glacial valley in North America, and one of the first examples of an upland alpine
51 glacial valley preserved in Earth's deep-time record.

52 **2 Geologic setting**

53 Unaweep Canyon is a large gorge that bisects Colorado's Uncompahgre Plateau, and is globally
54 unique, named for the odd occurrence of a divide in its midst, from which two creeks flow in
55 opposite directions (Fig. 1). The canyon incises through Mesozoic strata into Precambrian
56 basement but hosts a thick sediment fill of Pleistocene and possibly older age. It is overlapped by
57 Permian strata at its western mouth that bury up to ~520 m of paleorelief on Precambrian basement
58 (Soreghan et al., 2012, 2015). During the Pennsylvanian-Permian, the Uncompahgre uplift — a
59 large block uplift of the Ancestral Rocky Mountains that encompassed the greater Uncompahgre
60 Plateau and beyond — shed clastics into the Paradox Basin to the west-southwest. By Mesozoic
61 time, this region subsided, and accumulated substantial sediment before the Cenozoic uplift that
62 formed the modern Uncompahgre Plateau. During the latest Cenozoic, the ancestral Gunnison
63 River flowed through Unaweep Canyon, prior to its abandonment of the canyon (~1.4 Ma) and
64 partial backfilling (Balco et al., 2013; Soreghan et al., 2015).

65



67 **Figure 1.**

68 (a) Digital elevation model of Unaweep Canyon. UD: Unaweep Divide; MW: Massey well (core);
69 SP 2017: location of the seismic reflection profile (Fig. 2) in this study; pC: Precambrian
70 basement outcrops along the canyon floor. A-A': longitudinal cross-section shown in Fig. 4. v:
71 Viewpoint of (c). (b) Geologic map of the area shown in (a). (c) View into Eastern Unaweep
72 Canyon towards West. Indicated dimensions show horizontal distance of vertical basement cliffs
73 and vertical distance from plateau to the valley floor.

74

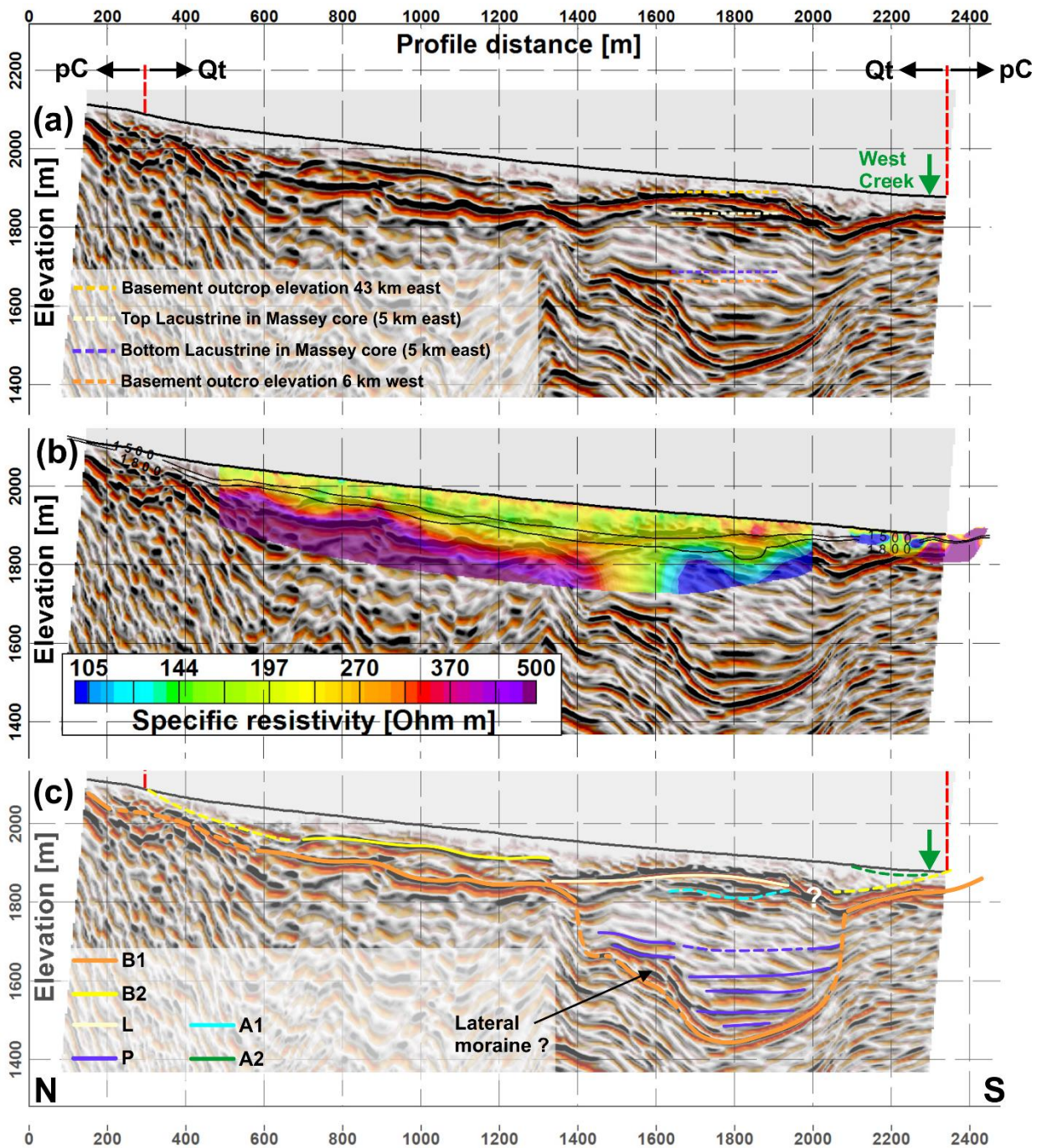
75 Although the most commonly accepted model for the formation of Unaweep Canyon is incision
76 by the ancestral Gunnison or Colorado river (e.g., Lohman, 1981; Aslan et al., 2008; Hood, 2009),
77 Soreghan et al. (2007, 2008, 2014, 2015) posited formation by late Paleozoic glaciation, followed
78 by Permian burial and Cenozoic partial exhumation by the ancestral Gunnison River. This
79 hypothesis remains controversial (e.g., Soreghan et al., 2008; Hood et al., 2009) since it implies
80 low-latitude and low-elevation glaciation for the late Paleozoic which is not a feature of current
81 climate models for that period. The hypothesis hinges in part on observations that suggest a pre-
82 Mesozoic age for the landform (e.g., burial of Permian paleorelief), and inferred proglacial facies
83 in the Permian fill, as well as a 320 m core that penetrated mostly Pleistocene strata but ~15 m of
84 basal strata interpreted to date from the late Paleozoic (Soreghan et al., 2008). Previous gravity
85 surveys (Soreghan et al., 2008) and electrical resistivity soundings (Oesleby, 1983) suggested
86 possible overdeepening of the Precambrian basement surface in the western canyon, but the
87 solutions are non-unique, hence the controversy persists.

88

89 **3 Methods**

90 A 2.45 km N-S seismic 2D reflection line was acquired across the widest part of Unaweep Canyon
91 (Fig. 1b, supplemental material S1). The acquisition comprised 505 receiver locations deployed
92 with nodal receivers and 264 shot locations. A truck-mounted impact hammer was used as the
93 primary energy source (Patterson, 2019). Raw data hint at basement deepening in the southern part
94 of the profile (S2). Data processing followed a standard workflow for 2D crooked line reflection
95 processing (e.g., Yilmaz 2001; S3). Intermediate processing products (NMO stack, pre-stack time
96 migration (PSTM), PSTM velocity model) strongly suggest a U-shaped basement surface (S4, S5),
97 and the final result is the depth-converted PSTM image (Fig. 2a).

98 Complementary measurements in this study correspond to a co-located electrical resistivity
99 tomography (ERT) profile (Fig. 2b). The data coverage gap at profile distance ca. 2000 m results
100 from logistical constraints, since the ERT cables could not be deployed across the intersecting
101 highway. Measurements were collected using an ARES II system (GF instruments) using 304
102 electrodes with a separation of 5 m. Measurements were collected with a Wenner-Gamma
103 configuration, with a maximum separation between current and potential dipoles of 125 times the
104 electrode spacing. To increase the signal-to-noise ratio for such readings, the ARES II unit permits
105 to use more than one electrode to form each pole of the current dipole. Inversion of the data was
106 carried out with CRTomo (by Kemna, 2000), a smoothness-constraint algorithm that solves the
107 Helmholtz equation in the wave number domain to calculate the distribution of the electrical
108 resistivity in an imaging plane. The inversion results converged to the measured resistances with
109 a data error of 5% relative error and 0.01 Ohm absolute error.



111

112 *Figure 2.*

113 (a) *Pre-stack seismic time migration (PSTM) image and ground-truth data. Pc, Qt: Precambrian*

114 *and quaternary surface cover. Dashed lines show elevations of basement outcrops (Fig. 1) along*

115 *UnawEEP Canyon and interpreted horizons in the Massey core. (b) Electrical resistivity*
116 *tomography image superimposed on the PSTM image. (c) Integrated interpretation of the PSTM*
117 *image, ground-truth data, and additional geophysical observables (supplemental material S5 –*
118 *S7). Dashed lines indicate where horizons are less well defined and/or are largely based on*
119 *supplemental data. B1: Consolidated Precambrian basement. B2: Top of Precambrian regolith*
120 *and pre-Quaternary sediments. L: Reflector associated with a Cenozoic lacustrine unit. P: pre-*
121 *Quaternary sediments. A1, A2: Top of deep and shallow aquifers.*

122

123 **4 Interpretation and discussion**

124 We conduct our interpretation (Fig. 2c) in depth instead of time to incorporate stratigraphy known
125 from a core located 5 km to the east ('Massey well'; Fig. 1) and additional geophysical data (S6 –
126 S8; Behm et al., (2019, 2020)). In absence of a well co-located with the seismic line, the PSTM
127 velocity model was used for depth conversion. The interpretation considers uncertainties of
128 seismic processing and imaging. Limitations in velocity model building and resolution can produce
129 small-scale 'migration smiles,' and depth conversion of time-migrated data without a well tie can
130 produce further lateral and vertical distortions. Seismic 2D cross-sections of distinct 3D structures
131 such as overdeepened valleys are prone to out-of-plane reflections which can further bias the
132 velocity model and the final image. Our interpretation also integrates additional geophysical data
133 (S6, S7) and the stratigraphic information from the distant Massey well core.

134 In the near surface (<150 m depth), the PSTM velocity model (S5) and the depth-converted
135 migrated image (Fig. 2) fit well with tomographic P-wave velocity inversion (S6), S-wave
136 velocities from surface wave inversion (S7), and the ERT data (Fig. 2b). In particular, the

137 deepening of the basement at profile distances 1400 m to 2100 m is qualitatively corroborated by
138 the lack of high P- and S-wave velocities and low electrical resistivity.

139 Horizon 'B1' represents consolidated Precambrian basement with P-wave velocities in the range
140 of 4500 to 5500 m/s (S6), suggesting a significant degree of weathering. Poor imaging between
141 profile distances 200 – 600 m relates in part to use of a weaker seismic source signal
142 (sledgehammer) necessitated by access limitations. At profile distances 1400 m and 2100 m, we
143 interpret abrupt and near-vertical descent of the basement surface. Between profile distances 1700
144 m and 2000 m, the basement surface forms a pronounced U-shape with a maximum depth of 490
145 m below the modern surface. This deepest point is also 220 m below the western basement outcrop
146 at 6 km lateral distance and therefore unambiguously establishes an overdeepened valley floor.
147 The horizontal distance between the vertical cliffs (~700 m) is comparable to the exposed basement
148 morphology in eastern Unaweep Canyon (Fig. 1c).

149 The consolidated basement is correlated with resistivities > 350 Ohm m. The overall moderate
150 basement resistivities (400 - 1000 Ohm m) suggest a significant amount of fluid-filled fractures
151 due to significant weathering.

152 Horizon 'B2' is clearly established in parts of the northern section of the profile only. Based on
153 the constraining surface geology, we infer it separates Quaternary cover from underlying
154 Precambrian regolith. The lower layer may also include a significant component of pre-Quaternary
155 shale or sandstones given its low resistivity (DR8).

156 In the overdeepened section, a continuous reflector ('L') appears at ca. 1850 m elevation between
157 profile distances 1300 m and 1900 m. This horizon approximates (within ~50 m) the top of a

158 lacustrine unit identified in the Massey core, recording a late Pleistocene lake resulting from a
159 river blockage ~1.4 Ma (Soreghan et al. 2007, 2015; Balco et al. 2013).

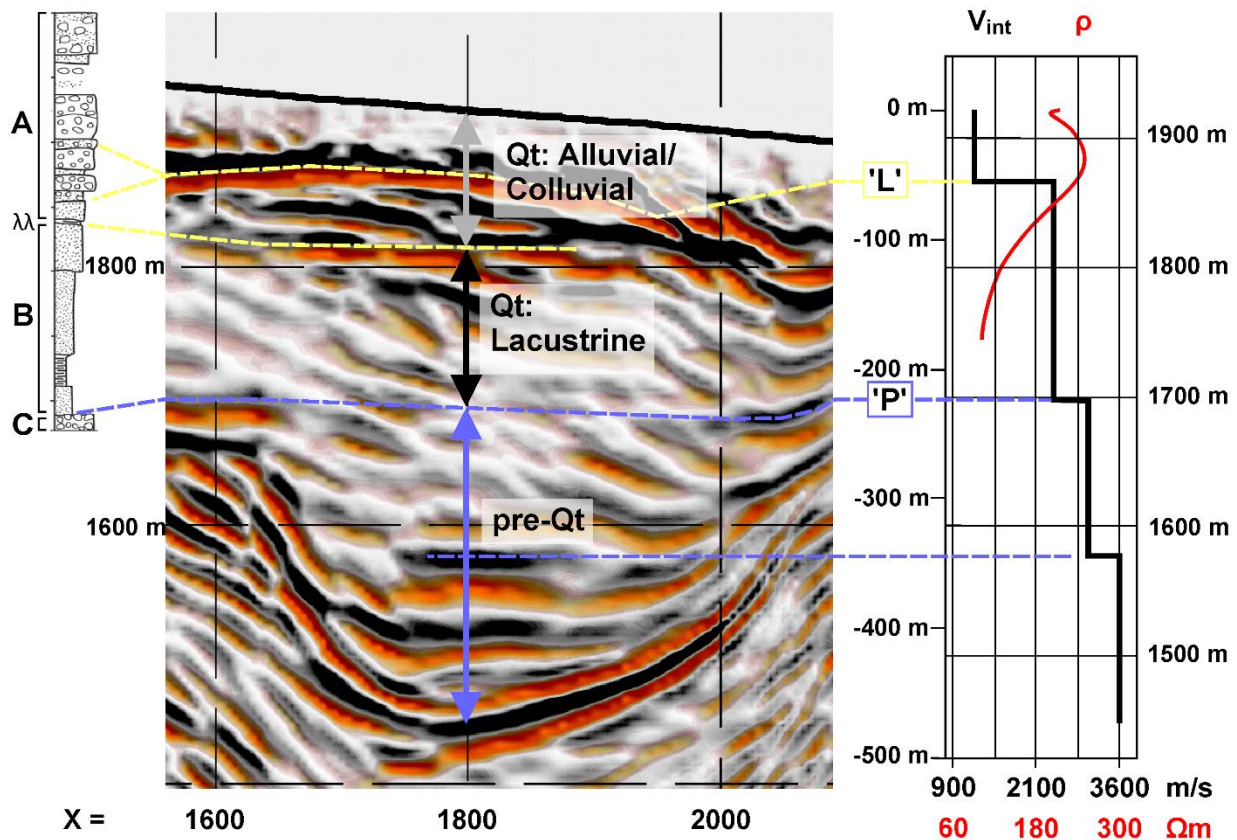
160 In the central part (profile distance 1700 – 2000 m) we associate increased reflectivity below ‘L’
161 with a strong drop in electrical resistivity (Fig. 2b), where resistivities < 120 Ohm m are interpreted
162 for aquifers in sand, suggesting the occurrence of an aquifer (horizon ‘A1’) in the lacustrine unit.
163 We also superimpose the 1500 m/s and 1800 m/s contour lines from the tomographic P-wave
164 velocity model (S6). Depending on the porosity, this velocity range is often taken as proxy for a
165 groundwater table in sand (Knight and Endres, 2005). It is noted that the apparent depression in
166 the resistivity structure (ca. profile distance 1850 m) correlates with the independently derived P-
167 wave velocity distribution. Accordingly, a shallow local aquifer in alluvium/colluvium (‘A2’)
168 could explain the low resistivity at West Creek (profile distance 2100 – 2300 m). Due to a gap in
169 the resistivity acquisition line, we cannot conclusively comment on a potential
170 connection/exchange between the two aquifers. However, it appears unlikely as the shallow
171 aquifer is related to West Creek situated at profile distance 2300 m.

172 Several horizontal reflectors (‘P’) appear in the overdeepened section between ca. 1670 m and
173 1480 m elevation. The shallowest one is apparent close to the basement cliffs, but images poorly
174 in the central part. This might relate to the aquifer ‘A1’, as water saturation of the lacustrine unit
175 increases seismic velocity and reduces the impedance contrast with underlying strata. Tilted and
176 basement-parallel reflectors with low interval velocities occur adjacent to and below ‘P’ (S5).

177 Fig. 3 shows a detail of the over-deepened section with the elevation-referenced stratigraphy of
178 the Massey core as well as the interval velocity and electrical resistivity extracted at the central
179 location of the seismic profile. We interpret the Pleistocene sediments to comprise ca. 100 m
180 colluvium and ca. 140 m lacustrine sand/silt. The top of the lacustrine unit ($\lambda\lambda$) might be

181 represented by the flat and weak impedance contrast below 'L'. Based on the correlation with the
 182 Massey core, we interpret the sequence below (reflectors 'P' in Fig. 2c) as pre-Quaternary strata
 183 with a total thickness of ~250 m.

184



185

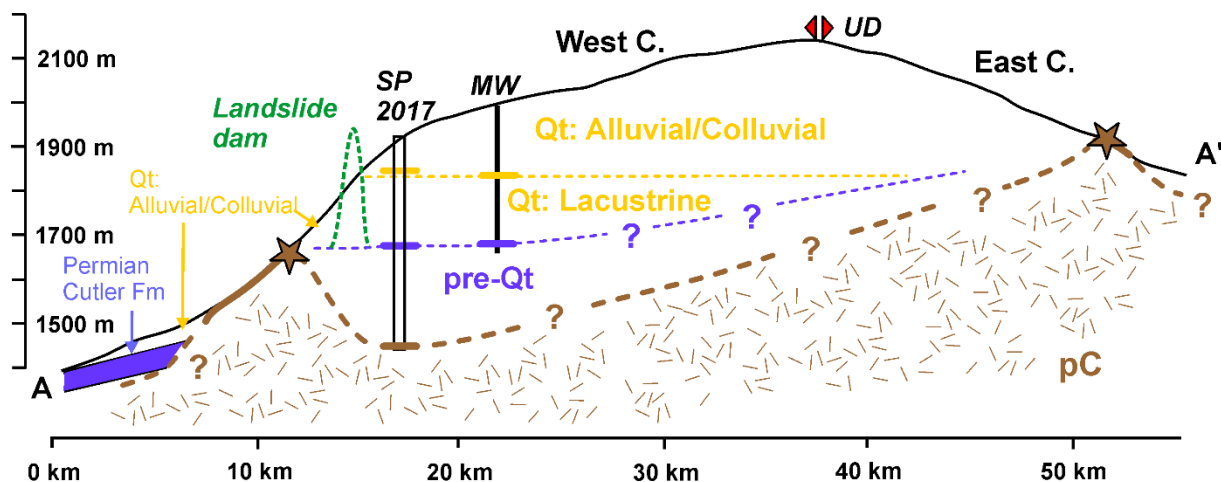
186 **Figure 3.**

187 *Correlation of the overdeepened section with the stratigraphy of the distant Massey core, interval*
 188 *velocities (V_{int}) and electrical resistivity (ρ). V_{int} and ρ are extracted at the central location $X=1800$*
 189 *m. Discrepancies in elevation are attributed to the approximate velocity model, the distance (5*
 190 *km) to the core, and lateral variation along the seismic section. Vertical axis represents elevation*
 191 *and depth below surface. 'L' and 'P' indicate top of interpreted reflectors as in Fig. 2b. Core*

192 sections after Balco et al. 2013: A – Qt Alluvium / Colluvium; λλ – Paleosoils; B – Qt Lacustrine;
 193 C – Pz Diamict

194

195 The integration of our interpretation with the stratigraphy of the Massey core and basement
 196 outcrops enables construction of a longitudinal section along the canyon (Fig. 4). The
 197 overdeepened character of the Precambrian basement surface of Unawep Canyon is
 198 unambiguous. The observed U-shape (cross-section) and the lack of faults of sufficient
 199 displacement to accommodate the overdeepening (Soreghan et al., 2015) strongly support a glacial
 200 origin. Bache et al. (2012) classified glaciogenic incision processes according to basement
 201 geometry and rock type. Given the depth, longitudinal and lateral extent and setting within
 202 crystalline basement, Unawep Canyon compares to the “alpine glacier” and “fjord” types. In that
 203 context, we speculate that the aforementioned tilted basal reflectors with low interval velocities
 204 might represent a lateral moraine (Fig. 2b), and that the lowermost stratified section of the valley
 205 fill could be indicative of a ground moraine.



206

207

208 *Figure 4.*

209 *Hypothesized vertical section along Unaweep Canyon following the dashed line in Fig. 1. Black*
210 *solid line: Topography along West and East Creek. UD: Unaweep Divide. MW: Massey well. SP*
211 *2017: Location of seismic profile. Dashed yellow line: Top of the lacustrine unit. Dashed purple*
212 *line: Top of pre-Quaternary strata. Dashed brown line: Overdeepened Precambrian basement.*
213 *Solid yellow/purple bars and brown lines show according observations from the seismic profile,*
214 *the well, and surface geology. Location of the 1.4 – 1.3 Ma landslide dam according to Balco et*
215 *al. 2013.*

216

217 Seismic interpretations of Paleozoic glacial valley fill in other parts of the world (Bache et al.
218 2012; Bataller et al. 2019) reveal complex stratigraphy representative of repeated glacier advances
219 and retreats, with additional complications arising from subsequent erosion, deformation, and
220 sedimentation events. Lack of a well penetration here precludes precise characterization of the
221 nature and age of the valley fill. We note however that the top of the pre-Quaternary strata aligns
222 with the fluvial base level of the ancestral Gunnison river 1.4 Ma ago (Balco et al., 2013; Soreghan
223 et al, 2015).

224 Soreghan et al. (2008) hypothesized that Unaweep Canyon was carved in the Late Paleozoic ice
225 age (LPIA). The modern elevation of the Uncompaghre Plateau, together with lack of evidence for
226 recent glaciation precludes Pleistocene glaciation here (Soreghan et al., 2007). The morphology of
227 the preserved bedrock surface, partial exhumation of a paleovalley at the western mouth of the
228 canyon, and the inferred proglacial facies of the Permian fill here all support the Paleozoic

229 hypothesis (Soreghan et al., 2009, 2015). Our results corroborate this hypothesis, implying that
230 Fig. 2 represents the first image of a glacial valley from a pre-Quaternary ice age in North America.
231 The accepted model for the late Paleozoic Ice Age (LPIA) holds that glaciation occurred across
232 the Gondwanan continents, at latitudes $>\sim 31^\circ\text{S}$ (Evans, 2003). In contrast, during the late
233 Paleozoic, the Uncompahgre uplift was within $\sim 11^\circ$ of the equator, and 60-80 km from the nearest
234 shoreline, implying that the paleoelevation near the contact between the Permian Cutler Formation
235 and Precambrian basement of the paleovalley was about ~ 1200 m elevation (Soreghan et al., 2014).
236 If this hypothesis is valid, then Unaweep Canyon represents a partially exhumed paleovalley
237 recording *upland* alpine glaciation — the first imaged example in Earth’s pre-Quaternary
238 equatorial record. Although the combination of all geological and geophysical observations favors
239 the late Paleozoic glaciation hypothesis, we cannot eliminate the possibility that Unaweep Canyon
240 preserves one or more Snowball Earth periods in the Neoproterozoic (Hoffman et al., 2017).
241 Determining between these options will require coring and dating of the over-deepened section.

242 **5 Conclusions**

243 Our results present the first high-resolution image of a buried paleovalley shaped by alpine
244 glaciation in Earth’s pre-Quaternary record. Combined with previously established evidence, the
245 most parsimonious explanation is that the Unaweep paleovalley was carved in the LPIA, at
246 relatively low elevations and low latitude, thus challenging climate models for that period, and
247 posing the question of how the paleoupland was preserved. Alternatively, the seismic image might
248 capture an even older (e.g. Neoproterozoic) glaciation. If Paleozoic, our results imply remarkable
249 preservation of an alpine glacial system, requiring subsidence of the ancestral Rocky Mountains
250 highlands immediately following their uplift. It furthermore suggests the possible existence of
251 additional buried paleovalleys atop the Uncompahgre Plateau, which might be imaged with

252 airborne geophysical tools (Pugin et al., 2014). Ultimately, our observations invite refinements in
253 climate modelling and motivate new field and modeling research in search of new evidence for
254 glaciations in other parts of the Carboniferous-Permian tropics.

255 **Acknowledgements**

256 The acquisition would not have been possible without the dedication of the field crew (P. Ratre,
257 F. Cheng, J. Chang, A. Eddy) and the expertise of G. Kaip and S. Harder (Seismic Source Facility,
258 UTEP). IRIS-PASSCAL provided Texan receivers. We thank Rick Lissoy and the Moores family
259 for property access and support and are indebted to the Gateway community for their hospitality.
260 Data were processed using software donations from Haliburton and Schlumberger. Acquisition
261 was partly funded through NSF-EAR-1338331 and NSF-EAR-1849623.

262 **Data Availability Statement**

263 Waveform data used in this study can be downloaded from Incorporated Research Institutions for
264 Seismology Data Management Center (IRIS-DMC) located at
265 <https://ds.iris.edu/SeismiQuery/assembled.phtml> through specifying the dataset name “Unawweep”
266 and the year “2017”.

267 **Supplemental Material**

268 Supplemental materials S1 – S7 can be found in the online version of this article.

269 **References**

270 Aslan, A., and 10 others (2008). River incision histories of the Black Canyon of the Gunnison and
271 Unawweep Canyon: Interplay between late Cenozoic tectonism, climate change, and drainage
272 integration in the western Rocky Mountains. In Reynolds, R.G. (ed.): Roaming the Rocky

273 Mountains and environs: Geological field trips: *Geological Society of America Field Guide* **10**,
274 175–202, doi: 10.1130/2008.fl.d010(09).

275 Bache, F., Moreau, J., Rubino, J. L., Gorini, C., Van-Vliet Lanoë, B. (2012). The subsurface
276 record of the Late Palaeozoic glaciation in the Chaco Basin, Bolivia. In Huuse, M., Redfern, J.,
277 Le Heron, D.P., Dixon, R.J., Moscariello, A., and Craig, J. (eds.): *Glaciogenic Reservoirs and*
278 *Hydrocarbon Systems*, Geological Society, London, *Special Publications* **368**,
279 doi:10.1144/SP368.11

280 Balco, G., Soreghan, G.S., Sweet, D.E., Marra, K.R., Bierman, P.R. (2013). Cosmogenic-nuclide
281 burial ages for Pleistocene sedimentary fill in Unaweep Canyon, Colorado, USA. *Quat.*
282 *Geochronol.*, **18**, 149–157

283 Bataller, F.J., McDougall, N., Moscariello, A. (2019). Ordovician glacial paleogeography:
284 Integration of seismic spectral decomposition, well sedimentological data, and glacial modern
285 analogs in the Murzuq Basin, Libya. *Interpretation*, **7**(2), T383–T408

286 Behm, M., Cheng, F., Patterson, A., Soreghan, G.S. (2019). Passive processing of active nodal
287 seismic data: estimation of V_p/V_s ratios to characterize structure and hydrology of an alpine valley
288 Infill. *Solid Earth*, **10**, 1337-1354

289 Behm, M., Flores-Orozco, A., Chwatal, W., Soreghan, G.S. (2020). Hydrologic characterization
290 of an alpine valley infill through integration of ERT, active seismic and active/passive surface
291 wave interferometry (Unaweep Canyon, US). Abstract EGU2020-6199 presented at 2020 EGU
292 Meeting, AGU, held online, 4-8 May

293 Bleibinhaus, F., Hilberg, S. (2012). Shape and structure of the Salzach Valley, Austria, from
294 seismic travelttime tomography and full waveform inversion. *Geophys. J. Int.*, **189**, 1701–1716

295 Brückl, E., Brückl, J., Chwatal, W., Ullrich, C. (2010). Deep alpine valleys: Examples of
296 geophysical explorations in Austria. *Swiss J. Geosci.*, **103**, 329–344

297 Burschil, T., Buness, H., Tanner, D.C., Wielandt-Schuster U., Ellwanger, D., Gabriell G. (2018).
298 High-resolution reflection seismics reveal the structure and the evolution of the Quaternary glacial
299 Tannwald Basin. *Near Surface Geophysics*, **16**, 593-610, doi: 10.1002/nsg.12011

300 Cook, S.J., Swift, D.A. (2012). Subglacial basins: their origin and importance in glacial systems
301 and landscapes. *Earth Sci. Rev.*, **115**(4), 332 - 372

302 Evans, D.A.D. (2003). A fundamental Precambrian– Phanerozoic shift in Earth’s glacial style?.
303 *Tectonophysics*, **375**, 353–385, [https:// doi .org /10 .1016 /S0040 -1951 \(03\)00345 -7](https://doi.org/10.1016/S0040-1951(03)00345-7)

304 Fiebig, M., Preusser, F., Decker, K., Schlüchter, C. (2010). Preface: Special section of papers
305 dealing with overdeepened basins and valleys in the alpine realm. *Swiss Journal of Geosciences*,
306 **103**, 327-328

307 de Franco. R., Biella, G., Caielli, G., Berra, F., Guglielmin, M., Lozej, A., Piccin, A., Sciunnach,
308 D. (2009). Overview of high resolution seismic prospecting in pre-Alpine and Alpine basins. *Quat.*
309 *Int.*, **204**, 65–75, doi:10.1016/j.quaint.2009.02.011

310 Hoffman, P.F., and 26 others (2017). Snowball Earth climate dynamics and Cryogenian geology-
311 geobiology. *Sci. Adv.*, **3**(11), p. e1600983, doi: DOI: 10.1126/sciadv.1600983

312 Hood, W.C., Cole, R.D., Aslan, A. (2009). Anomalous cold in the Pangaean tropics – Comment.
313 *Geology*, **37**(6), e192. doi: 10.1130/G30035C.1

314 Hooke, R.L. (1991). Positive feedbacks associated with erosion of glacial cirques and
315 overdeepenings. *Geological Society of America Bulletin*, **103**, 1104-1108.

316 Kemna, A. (2000). Tomographic inversion of complex resistivity - theory and application [Ph.D.
317 thesis], Bochum, Ruhr-University, 196 p.

318 Knight, R. J., Endres, A. L., (2005). An Introduction to Rock Physics Principles for Near-Surface
319 Geophysics. In Butler, D. (ed.), *Near Surface Geophysics*, Tulsa, Society of Exploration
320 Geophysicists

321 Lohman, S.W. (1981). Ancient drainage changes in and south of Unaweep Canyon, southwestern
322 Colorado. In Epis, R.C., and Callender, J.F. (eds.), *Western Slope Colorado. New Mexico*
323 *Geological Society Guidebook 32*: New Mexico Geological Society, Socorro, NM, 137-143.

324 Oesleby T.W. (1983). Geophysical measurement of valley-fill thickness in Unaweep Canyon,
325 west-central Colorado. In Averett W.R. (ed.): *Northern Paradox Basin, Uncompahgre Uplift field*
326 *trip guidebook*: Grand Junction, Colorado Grand Junction Geological Society 71– 72.

327 Patterson, A. (2019). Reflection seismic investigation of an alpine valley in Unaweep Canyon,
328 Western Colorado: Evidence of paleozoic glaciation of the Uncompahgre plateau [M.Sc. thesis],
329 Norman, University of Oklahoma, 95 p.

330 Pomper, J.E., Salcher, B.C., Eichkitz, C., Prasicek, G., Lang, A., Lindner, M., Götz, J. (2017). The
331 glacially overdeepened trough of the Salzach Valley, Austria: Bedrock geometry and sedimentary
332 fill of a major Alpine subglacial basin. *Geomorphology*, **295**, 147–158

333 Preusser, F., Reitner, J.M., Schlüchter, C. (2010). Distribution, geometry, age and origin of
334 overdeepened valleys and basins in the Alps and their foreland. *Swiss Journal of Geosciences*, **103**,
335 407-426

336 Pugin, A. J. M., Oldenborger, G. A., Cummings, D. I., Russell, H. A. J., Sharpe, D.R. (2014).
337 Architecture of buried valleys in glaciated Canadian Prairie regions based on high resolution
338 geophysical data. *Quat. Sci. Rev.*, **86**, 13–23.

339 Soreghan, G.S., Sweet, D.E., Marra, K.R., Eble, C.F., Soreghan, M.J., Elmore, R.D., Kaplan, S.A.,
340 Blum, M.D. (2007). An exhumed late Paleozoic Canyon in the Rocky Mountains. *Journal of*
341 *Geology*, **115**, 473-481.

342 Soreghan, G.S., Soreghan, M.J., Poulsen, C.J., Young, R.A., Eble, C.F., Sweet, D.E., Davogusto,
343 O.C. (2008). Anomalous Cold in the Pangaeian Tropics. *Geology*, **36**, 659–62.

344 Soreghan, G.S., Keller, G.R., Gilbert, M.C., Chase, C.G., Sweet, D.E. (2012). Load-induced
345 subsidence of the Ancestral Rocky Mountains recorded by preservation of Permian landscapes.
346 *Geosphere*, **8**(3), 654–68, doi: 10.1130/GES00681.S1

347 Soreghan, G.S., Sweet, D.E., Heavens, N.G. (2014). Upland glaciation in tropical Pangaea:
348 Geologic evidence and implications for climate modeling. *Journal of Geology*, **122**, 137-163.

349 Soreghan, G.S., Sweet, D.E., Thomson, S.N., Kaplan, S.A., Marra, K.R., Balco, G., Eccles, T.M.
350 (2015). Geology of Unaweep Canyon and its role in the drainage evolution of the northern
351 Colorado Plateau. *Geosphere*, **11**(2), 320–41, doi: 10.1130/GES01112.1

352 Yilmaz, O. (2001). *Seismic Data Analysis: Processing, Inversion, and Interpretation of Seismic*
353 *Data*: Tulsa, Society of Exploration Geophysicists, 2065 p.

354

Supplemental material to Patterson et al. “**Seismic reflection and electrical resistivity imaging reveals pre-Quaternary glaciation in the Rocky Mountains (Unaweep Canyon, Colorado)**”

Figure S1 (next page): Map view of the acquisition. Grid coordinates are in UTM Zone 12N.

Cyan line: Three-component 5 Hz Fairfield ‘ZLand’ seismic recorders at 5 m spacing (120 stations). Blue line: One-component 4.5 Hz Reftek ‘Texan’ seismic recorders at 5 m spacing. Grey dots: Manual sledge hammer source locations at 10 m spacing. Red dots: Nitrogen-pressured impact source A200 locations at 10 m / 5 m spacing. Yellow dashed line: Location of the vertical projection plane used in Figs. 2,3, DR5 – DR8. Labels indicate profile distance (in meters) shown in those figure axes. Qt, pC: Quaternary and Precambrian surface cover. White lines: Elevation contours (m).

A detailed description of the survey layout is provided in Patterson (2019).

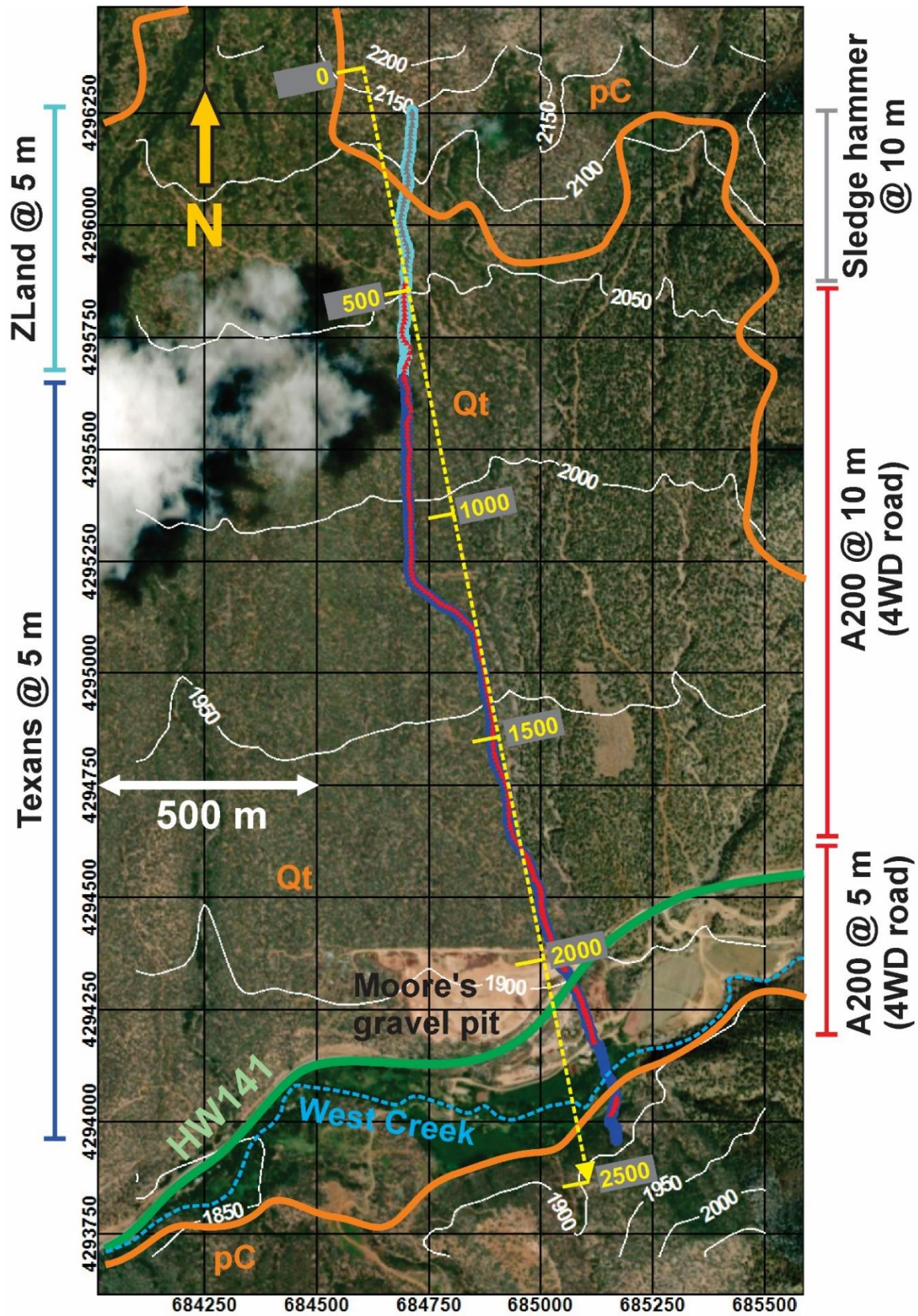
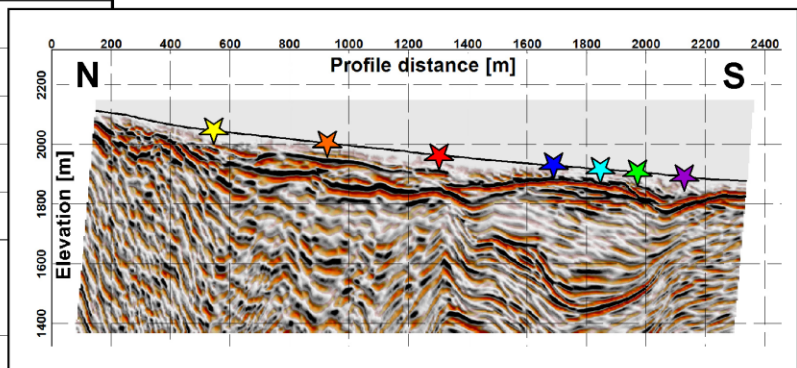
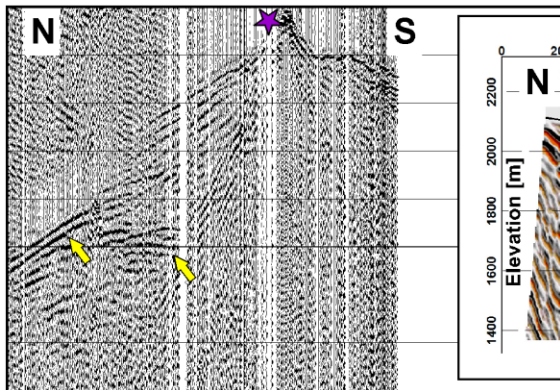
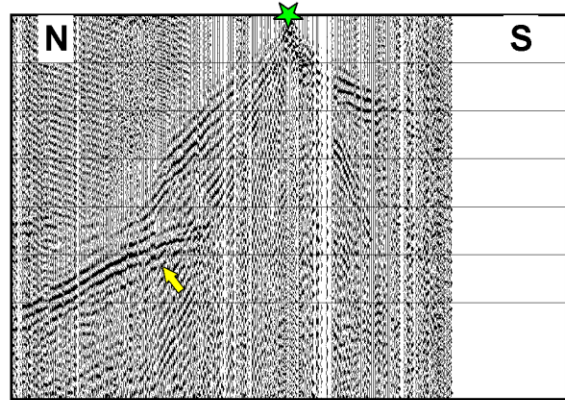
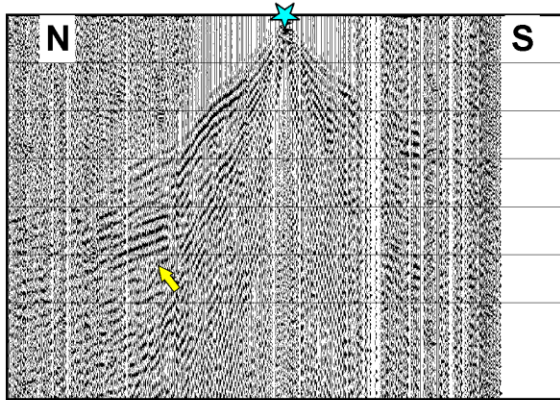
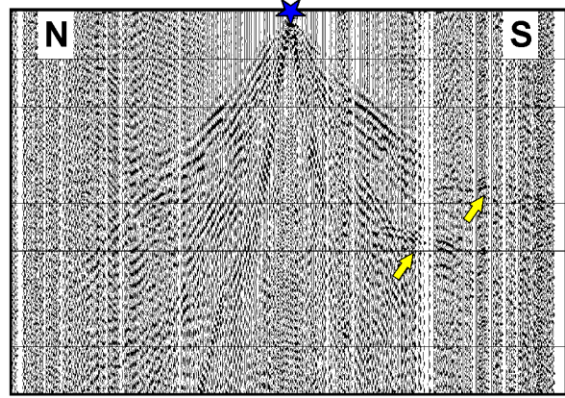
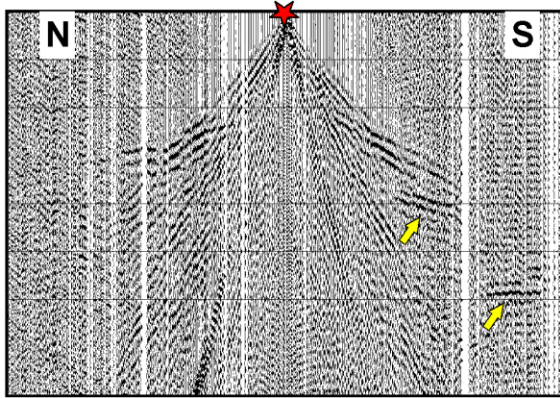
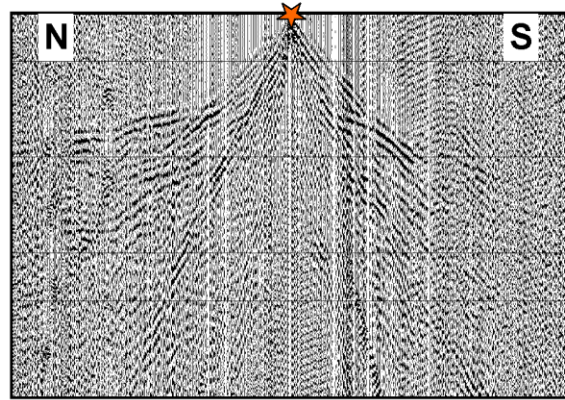
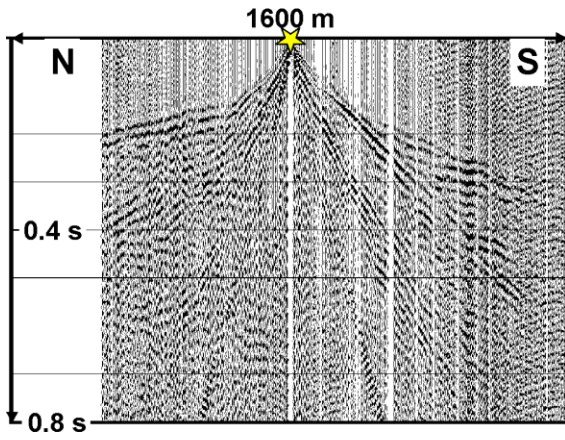


Figure S2 (next page): Selected shot gathers (raw data) along the profile after application of a bandpass filter (30 – 60 – 130 – 160 Hz) and AGC with 500 ms window length. Vertical and lateral extent is identical for all shot gathers (+/- 800 m offset, 0.8 seconds recording time). The colored stars correspond to the shot locations at the profile shown in the PSTM image. The yellow arrows highlight asymmetric and skewed reflection arrivals and are indicative of a complex subsurface structure with sudden changes in basement depth.



Data have been processed independently with Haliburton ProMAX and SLB Vista, providing similar results in terms of subsurface structure and velocities. The final results are from the Vista processing sequence, which turned out to image the data slightly better.

1. Trace editing, crooked line geometry application, CMP binning (bin size 5 m)
2. First arrival picking, elevation and refraction statics, reduction to floating datum
3. Initial Signal processing: Bandpass filter (10-25-90-130 Hz), AGC (window length 250 ms), notch filters, FK filter, Top and bottom mute
4. Predictive Deconvolution: Operator length 120 ms; Prediction lag = second zero crossing of the autocorrelation, taper length 20 ms, pre-whitening 2%
5. CMP sorting and velocity analysis: Super gathers of 10 CMP bins, offset restriction 150 – 950 m, bandpass filter 10-15-80-100 Hz
6. Velocity model smoothing
7. NMO stack: Offset restriction 100 – 600 m, stack normalization by the square root of the number of traces, stretch mute 100%*
8. Residual power statics calculation and application, new NMO stack (Fig. DR4)
9. Iterative PSTM velocity and PSTM aperture angle analysis
10. Velocity model smoothing
11. PSTM: Offset restriction 100 – 600 m, rephasing filter, stack normalization by the square root of the number of traces, anti-alias filter 15-75 Hz, stretch mute 100%*(Fig. DR4)
12. Depth conversion with the smoothed PSTM velocity model
13. Bandpass filter (10-15-65-80 Hz), AGC (window length 300 ms), mean scaler, trace mix (weights 1-3-1) (Fig. 2)

*: A large stretch mute was required to image the shallow basement ‘B1’ in the left part of the profile and the reflector ‘L’. We attribute this uncommonly high value to a large velocity gradient in the sedimentary cover above the reflectors, which causes reflection rays to arrive at larger offsets.

Table S3: Processing sequence and parameters

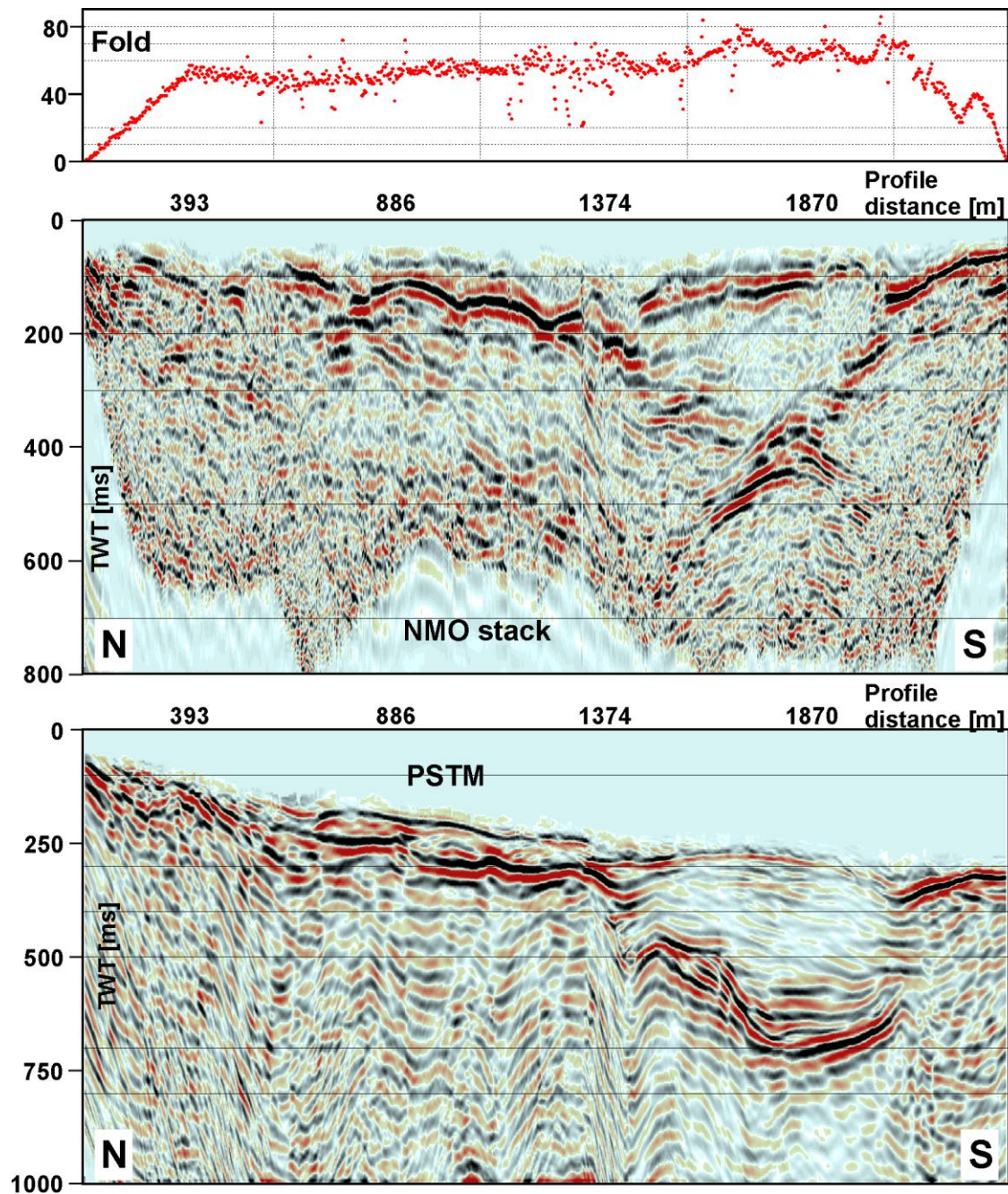


Figure S4: NMO stack referenced to the floating datum with corresponding fold, and PSTM image referenced to the final datum. The fold scatters is due to the crooked line bins. The stack clearly shows significant overdeepening and is indicative of a U-shaped structure (e.g., compare to de Franco et al., 2009, Figs. 3 and 5). The superposition of the horizontal reflectors and the diffraction hyperbola (profile distances 1400 – 1900 m) illustrates the necessity of pre-stack time migration. Both NMO stack and PSTM image are bandpass filtered (10-15-65-80 Hz) and scaled with AGC (window length 500 ms)

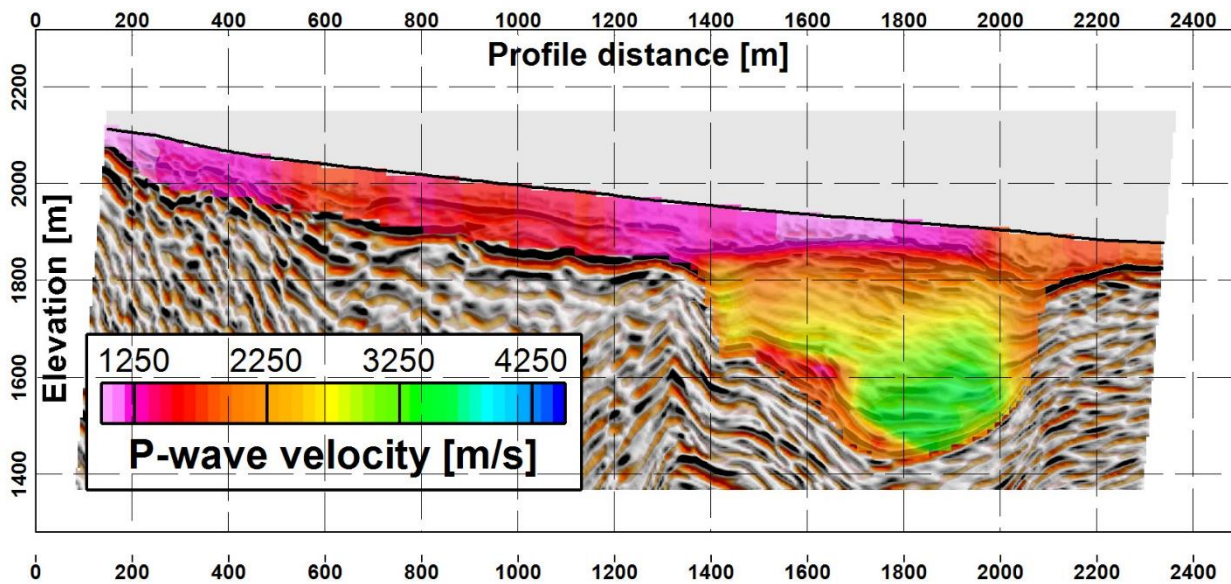


Figure S5: Smoothed and depth-converted PSTM interval velocity model. In absence of a local well, this velocity model was also used for the time-to-depth conversion of the PSTM image.

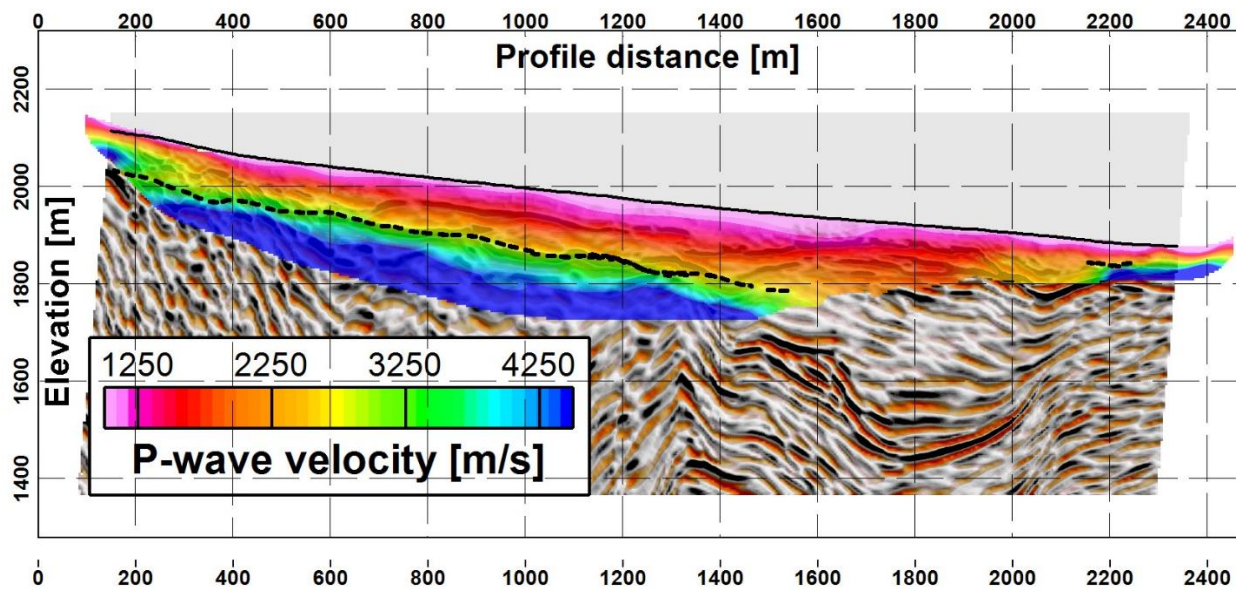


Figure S6: Tomographic velocity model and refractor depth (black dashed line) based on first arrival travel times (see Behm et al., 2019 for details). The lack of basement rock velocities (> 4000 m/s) and the absence of a well-defined refractor coincides with the area of overdeepening (profile distance 1500 – 2100 m). Tomographic velocities and refractor depth were established independently from reflection processing.

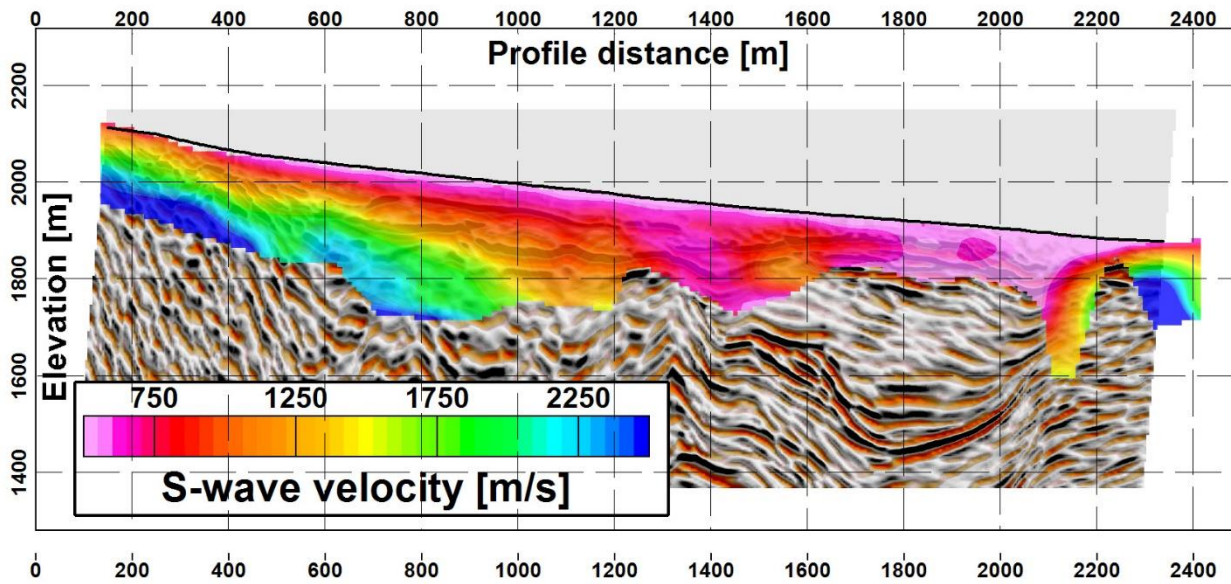


Figure S7: Shear wave velocity model based on surface wave inversion (see Behm et al., 2019 for details). The low velocities in the deeper section are indicative of significantly weathered basement rock. The resolution and accuracy of surface wave inversion is in general inferior to travel time tomography, but nonetheless we observe a similar structure as in figures 2, S5, and S6 (shallowing of basement towards the north, sudden change from deep basement to shallow basement at profile distance ca. 2100 m).